BAUET JOURNAL
Published by
Bangladesh Army University of Engineering & Technology (BAUET)
Journal Homepage: https://journal.bauet.ac.bd/
DOI: https://doi.org/10.59321/BAUETJ.V5I1.2

High-Performance Plasmonic Biosensor using Monocore Photonic Crystal Fiber for Biological and Chemical Detection

Md. Abdullah Al-Moti Pinto[1*], Md. Rubel Basar[1], Md. Saiful Islam[1], Tanvir Ahmed[2]

[1]Department of Electrical and Electronic Engineering, Bangladesh Army University of Engineering &Technology (BAUET), Qadirabad Cantonment, Natore-6431, Bangladesh
[2]Department of Electrical and Electronic Engineering, Faculty of Electrical & Computer Engineering, Rajshahi University of Engineering & Technology, Rajshahi-6204, Bangladesh

Abstract: Plasmonic biosensors have gained substantial attention for their potential in real-time, label-free detection of biological and chemical analytes, particularly in medical diagnostics and environmental monitoring. In this work, we proposed a highly sensitive surface plasmon resonance (SPR)-based biosensor employing a monocore photonic crystal fiber (PCF) with a gold-coated outer surface. In contrast to traditional dual-core PCF designs, the proposed structure employs a compact single-core geometry with a gold plasmonic layer coated on the outer surface which can simplify the fabrication process while preserving strong light–plasmon interaction. The sensor's optical performance is investigated using the finite element method (FEM) that reveals the maximum wavelength sensitivity of 18,000 nm/RIU, the amplitude sensitivity of 3012 RIU^{-1}, and the resolution of 5.6×10^{-6} RIU across the analyte refractive index (RI) range of 1.33 to 1.42. These results highlight the sensor's high accuracy, broad detection range, and robust design, making it a strong candidate for real-time biological and biochemical sensing applications.

Keywords: *Surface Plasmon Resonance (SPR); Photonic Crystal Fiber (PCF); Monocore PCF; Gold-coated PCF*

Introduction: The use of surface plasmon resonance (SPR) has become as a powerful optical sensing strategy, offering label-free and highly sensitive real-time detection. This has positioned SPR-based sensors as essential tools in diverse applications ranging from biomedical diagnostics to biochemical analysis. Ritchie's 1957 theory of surface plasmon energy loss in thin films laid the foundation for the prism-coupled SPR technique developed by Kretschmann and Raether in 1968, now widely used in biosensing. While prism-coupled configurations offer precise measurements, their bulky and mechanically complex nature limits their integration into compact system[1], [2].

To overcome these challenges, Jorgenson and Yee proposed utilizing optical fibers coated with plasmonic materials as a more compact and adaptable platform for SPR sensing[3]. The integration of photonic crystal fibers (PCFs) enhances SPR sensor capabilities by enabling precise control of light propagation. Their high birefringence, strong light confinement, low interference, and broad single-mode operation make them ideal for applications in chemical sensing, environmental monitoring, virus detection, and medical diagnostics [4]. In designing SPR sensors, silver and gold, two noble metals, are frequently selected due to their ability to sustain surface plasmon waves. Silver typically offers stronger plasmonic activity, which can lead to higher sensitivity in detection. However, its tendency to oxidize under normal environmental conditions limits its durability for long-term use. Gold, by contrast, exhibits excellent chemical stability and compatibility with biological environments, making it a more reliable material for practical and reusable biosensing systems [5]. Additionally, the adoption of gold layers on the outer surfaces of PCF structures has been found to simplify fabrication while maintaining effective interaction with the analyte [6].

Building upon this foundational understanding, recent developments in SPR-based PCF sensor designs have primarily focused on improving performance indicators such as sensitivity, resolution, and detection range. For instance, Li et al. [7] designed a sensor achieving 641 RIU^{-1} in amplitude sensitivity and 11,000 nm/RIU in wavelength sensitivity within a refractive index range covering from 1.350 to 1.395. Chakma et al. [8] proposed a sensor using gold coating made from fused silica with sensitivities of 318 RIU^{-1} and 9000 nm/RIU. Rifat et al. [6] presented a sensor with an exterior gold coating that has a resolution of 3.75×10^{-5} RIU and a sensitivity of 2200 nm/RIU. The field has continued to progress with additional varieties. A ring-shaped PCF with an exterior gold coating was used by Zhou et al. [9], producing wavelength sensitivity 6900 nm/RIU and amplitude sensitivity 132 RIU^{-1}, respectively. Hasan et al. [10] enhanced performance further using a layered configuration of gold and niobium with Al_2 O_3, resulting in up to 8000 nm/RIU wavelength sensitivity and 1560 RIU^{-1} amplitude sensitivity. A dual-core configuration proposed by Paul et al. [11] reached 11,500 nm/RIU and 636.5 RIU^{-1} and a noticeable resolution of 8.7×10^{-6} RIU. In addition, Sarkar et al. [12] demonstrates a nanoscale externally gold coated sensor with reported wavelength sensitivity of 9000 nm/RIU, amplitude sensitivity of 1902 RIU-1 and a RI detection range of 1.32 to 1.40.

Article history:
Received 12 June 2025
Received in revised form: 10 October 2025
Accepted 15 November 2025
Available online 15 December 2025

Corresponding author details: Md. Abdullah Al-Moti Pinto
E-mail address: abdullahalmotipinto@gmail.com
Tel: +8801768222610

Inspired by these advancements, this work presents a compact SPR biosensor using a monocore PCF with a hexagonal lattice configuration. The design strategically omits specific air holes to establish a central core, enhancing birefringence and improving overall light-matter interaction. The sensor's geometrical parameters lattice pitch, air hole dimensions is optimized to achieve superior sensitivity and performance across a broad range of refractive indices of sensing medium. As compare to previous monocore or externally coated designs, the proposed sensor demonstrates excellent performance, achieving a superior wavelength sensitivity of 18000 nm/RIU, an amplitude sensitivity of 3012 RIU^{-1}, a wide detection range from RI 1.33 to RI 1.42, and a remarkable resolution of 5.6×10^{-6} RIU. A gold layer as plasmonic material has been coated across the surface of the PCF structure and the analyte layer has been positioned with the plasmonic layer. A PML layer also used to absorb the reflections.

Model Structure and Geometrical Definition: Fig. 1(a) shows the suggested sensor's cross-sectional geometry. A hexagonal lattice with a pitch denoted by Λ (distance between two adjacent air holes) of 2 µm. To create the solid core, all the air holes from the middle of the PCF structure are purposefully omitted. In order to create a sensing channel and enable light transmission toward the metal-analyte contact, air holes of the outer ring are eliminated also. Strong evanescent field interaction with the surface plasmon polariton (SPP) at the plasmonic material-dielectric interface has been made possible by this open region, which improves sensing effectiveness. Two distinct diameters of air holes are present in the outer ring: bigger holes with diameter d_1 = 0.8 × Λ and smaller holes with diameter d_2 = 0.3 × Λ. The core region's light confinement is enhanced by these air holes, and the birefringence properties are strengthened by the smaller air holes that line up with the locations of the outer ring's missing holes. A consistent layer of gold, 40 nm thick, is applied around the sensor structure to serve as the plasmonic interface. Adjacent to this metallic layer is the sensing medium, or analyte, which occupies a 1.7 µm thick region. A perfectly matched layer (PML) of 1.7 µm is introduced outside the sensing zone to guarantee numerical stability and suppress false reflections at the domain boundaries during FEM simulation. The PCF structure is typically fabricated by constructing a preform and utilizing a regular drawing tower to draw the fiber in a high-temperature furnace.

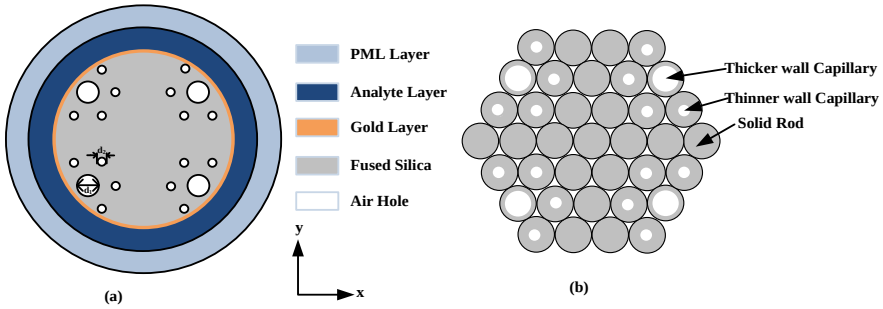

Fig. 1: Proposed monocore PCF-based SPR sensor: (a) Cross-sectional view and (b) Schematic of the stacked preform.

The preform is created by stacking silica capillaries and rods in a controlled arrangement, commonly referred to as the stack-and-draw method [13]. Optical guiding regions are engineered by introducing structural modifications, such as replacing capillaries with solid rods or omitting them altogether, which directly affects modal characteristics [14]. Air holes of varying sizes are introduced using capillaries of different wall thicknesses, as shown in Fig. 1(b). The most critical step in fabrication process is coating or deposition of plasmonic metal layer on the main PCF structure. While various coating techniques exist, many involve elevated temperatures that may adversely affect the structural integrity of the fiber. To address this concern, electron beam evaporation is adopted as it provides uniform coating under vacuum conditions at relatively low temperatures. This technique is ideal for plasmonic sensor applications since it provides exact control over the deposited gold film's thickness and quality [15].

Silica glass serves as the PCF's background material in this investigation. The Sellmeier equation is widely utilized to ascertain its refractive index, that accurately models the wavelength-dependent dispersion characteristics of silica [16]. The Drude-Lorentz model is utilized to determine the permittivity of the metal, gold, which acts as the plasmonic layer, as a function of wavelength can be determined using eq. 1 [17]:

$$\varepsilon_{Au} = \varepsilon_{\infty} - \frac{\omega_D^2}{\omega(\omega + j\gamma_D)} - \frac{\Delta\varepsilon\Omega_L^2}{(\omega^2 - \Omega_L^2) + j\Gamma_L\omega} \quad \text{eq.1}$$

where, ε_{Au} = permittivity of gold, ε_{∞} = 5.9673 (permittivity at high frequency), $\omega = {}^{2\pi c}/_{\lambda}$ (The angular frequency), ω_D = plasma frequency, γ_D= damping frequency respectively, whereas $\frac{\omega_D}{2\pi} = 2113.6\,THz$ and $\frac{\gamma_D}{2\pi} = 15.92\,THz$, $\Delta\varepsilon = 1.09$ (weighting factor) while $\frac{\Gamma_L}{2\pi} = 104.86\,THz$ and $\frac{\Omega_L}{2\pi} = 650.07\,THz$ are the spectral width and oscillator strength of the Lorentz oscillators, respectively.

In order to simulate the proposed sensor, a homogenous dielectric medium is used in analyte layer, which is situated just above the gold covering. A numerical analysis is conducted using the finite element method (FEM) performed in COMSOL

Multiphysics to assess the optical performance of the suggested sensor. A physics-controlled mesh with fine element size is employed to ensure the resolution accuracy at the plasmonic layer in the metal dielectric interface. The entire domain consists of triangular size element with an element distribution: 27,072 triangular elements, 2,066 boundary (edge) elements, and 96 vertex elements. The mesh settings automatically refine the mesh element size in the high field- gradient region like metal- analyte interface while maintaining a coarser mesh in the low field-gradient region to optimize computational efficiency. We used the convergence criterion in this simulation to compare the results obtained with different mesh densities such as coarse, fine, and extra-fine meshes. The resonant wavelength difference for fine and extra fine meshes is found less than 0.1 nm, confirming the numerical stability and convergence. Therefore, fine mesh is used for entire simulation results. To ensure precise calculation of the guided and surface plasmon modes, a perfectly matched layer (PML) in circular shape is deployed at the simulation domain's outer border to absorb outgoing radiation and remove spurious reflections. Since the PCF's geometrical configuration has a significant impact on the sensor's performance. Therefore, the design parameters are selected to enhance the interaction between the evanescent field and the plasmonic metal interface, which is crucial for effective SPR excitation. These parameters are also chosen with fabrication feasibility in mind. In this sensor the SPR occurs when incident light couples with free electrons at the metal-dielectric interface, leading to the generation of surface plasmon waves. This resonance condition arises when the propagation constants of the core-guided mode and the SPP mode become equal. At resonance, a distinct loss peak appears in the transmission spectrum, and variations in the analyte's refractive index can be detected by monitoring shifts in the peak's amplitude or wavelength. Due to the birefringence introduced by the asymmetric structure of the hexagonal lattice, the proposed sensor supports two fundamental polarization modes.

Performance Analysis of Proposed Sensor: A comprehensive simulation was conducted to analyze the proposed sensor's performance. The significance of results is discussed in this section. Fig. 2 shows the distributions of electric field confirm the sensor's ability to support polarization-dependent coupling, which can be exploited to improve sensitivity and detection resolution. The exponentially high sensitivity of the sensor is obtained from the engineered geometry of the proposed structure. The presence of multiple air holes in the cladding region effectively reduces the effective mode index of the PCF compared to conventional designs. As a result, the Transverse Magnetic (TM) polarized light can penetrate deeper into the metal layer that maximizes the coupling of core mode and SPP mode. The intensity map clearly shows that a high energy concentration adjacent to the plasmonic layer confirms a strong light-matter interaction. Because of a large optical power resides within the plasmonic layer, a tiny change in the analyte refractive index can significantly perturbs the propagation constant of SPP. For this strong perturbation, shifting in resonant wavelength is amplified, leading to a high wavelength sensitivity of 18000 nm/RIU. Moreover, enhanced field confinement at the metal boundary creates a high absorption of light in resonant conditions. The rapid change in loss due to changes in analyte RIs creates a high amplitude sensitivity of 3012 RIU^{-1}. The combined effect of optimized plasmonic confinement, deep evanescent field penetration and maximized overlap of core and SPP modes creates a high resonance dip and sharp resonant wavelength shift per RI change, resulting in a low detection resolution of 5.6×10^{-6} RIU.

Fig. 3 illustrates the dispersion characteristics of the presented PCF sensor for a single analyte with refractive index 1.40 over the wavelength from 750 nm to 850 nm. The spectrum of confinement loss is represented by the dark red solid line, while the real parts of the effective refractive indices for the core-guided modes are plotted using dotted blue lines and SPP modes are plotted using solid blue lines, respectively. A prominent resonance is found around the wavelength of 800 nm, where the effective indices of the core and SPP mode converge. This convergence point indicates phase matching between the core mode and the SPP mode, facilitating efficient energy coupling. As a result, a pronounced peak appears in the confinement loss curve at this wavelength.

The confinement loss α, measured in decibels per centimeter (dB/cm), is computed using eq. 2 [18]:

$$\alpha = 8.686 \times {}^{2\pi}/_{\lambda} \times Im[\eta_{eff}] \times 10^{4} \quad \text{(dB/cm)} \qquad \text{eq. 2}$$

A strong wavelength-dependent loss profile is observed in the x-polarized mode as the analyte refractive index varies. With the variation of refractive indices from 1.33 to 1.42, the resonance wavelengths shift progressively from 590 nm to 1070 nm, indicating a consistent redshift with increasing RI values. This behavior reflects the effective coupling condition between guided core mode and SPP mode for each RI level. The full spectrum of resonance shifts is depicted in Fig. 4.

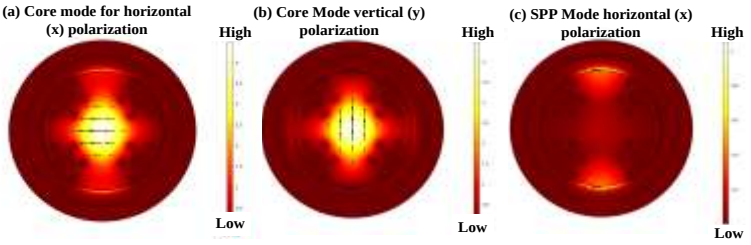

Fig. 2: Electric field distribution in the proposed sensor for (a) core mode x-polarization, (b) core mode y-polarization, (c) SPP mode x-polarization.

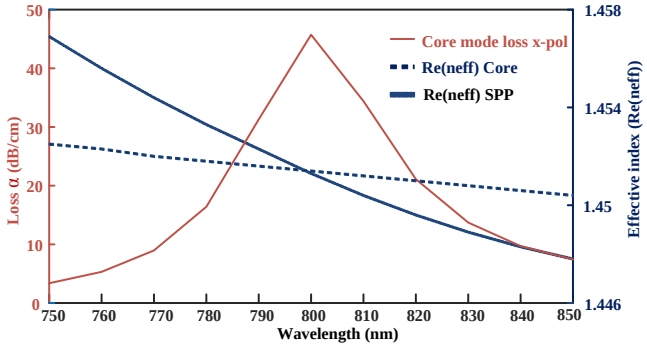

Fig. 3: The dispersion characteristics for analyte refractive index 1.40.

Fig. 5 illustrates the connection between the analyte RI and the resonant wavelength. A polynomial fit reveals a significant correlation with an R^2 value of 0.9715, showing strong linearity. The linear response of the sensor is further supported by the slow shift of the resonance wavelength toward longer wavelengths as RI increases. The figure of merit (FOM) serves as a key performance indicator, balancing wavelength sensitivity against the spectral bandwidth of the resonance peak. It can be determined as the ratio of the sensor's wavelength sensitivity to the full width at half maximum (FWHM) of the confinement loss curve. A higher FOM reflects enhanced detection precision. In the case of the proposed sensor, the maximum FOM (Fig. 6) is reported as 458 at a refractive index of 1.41, indicating excellent sensitivity with a sharp resonance behavior. Another key parameter for measurement of the performance of the sensor is amplitude sensitivity S_A, calculated using the amplitude interrogation method. This parameter quantifies how significantly the loss changes with variation in the analyte's RI.

The amplitude sensitivity S_A is determined as a function of the propagation loss $\alpha(\lambda, n_a)$ using eq. 3 [19].

$$S_A(\mathrm{RIU}^{-1}) = -\frac{1}{\alpha(\lambda, n_a)} \frac{\delta\alpha(\lambda, n_a)}{\delta n_a} \qquad \text{eq. 3}$$

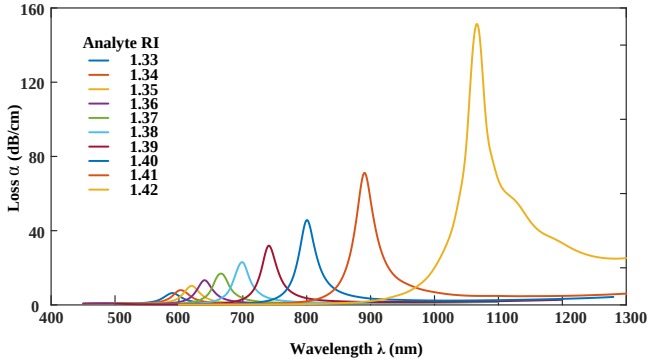

Fig. 4: Loss spectra of the proposed SPR sensor for analyte refractive indices ranging from 1.33 to 1.42.

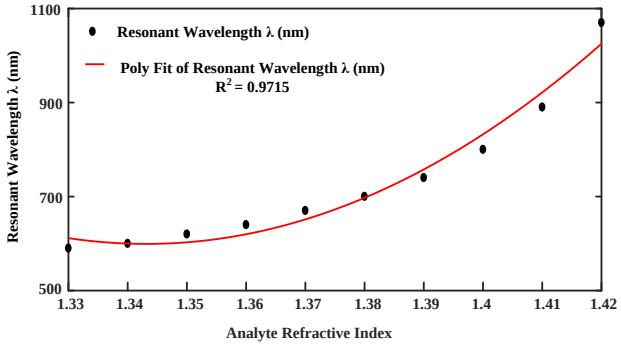

Fig. 5: Resonance wavelength shifts as a function of analyte refractive index (1.33–1.42) for x-polarized light, with polynomial fitting (R^2 = 0.9715).

Fig. 7 presents the amplitude sensitivities for x-polarized light across analyte refractive indices ranging from 1.33 to 1.41, with values increasing from 138 to a peak of 3012 RIU^{-1}. The highest sensitivity 3012 RIU^{-1} is recorded at a wavelength of 1070 nm, demonstrating the sensor's enhanced performance in the near-infrared region. The wavelength sensitivity $S(\lambda)$ measured in unit nm/RIU can be determined using the following eq. 4 based on [18]

$$S(\lambda) = \frac{\delta\lambda_{peak}}{\delta n_e}, \qquad \text{eq. 4}$$

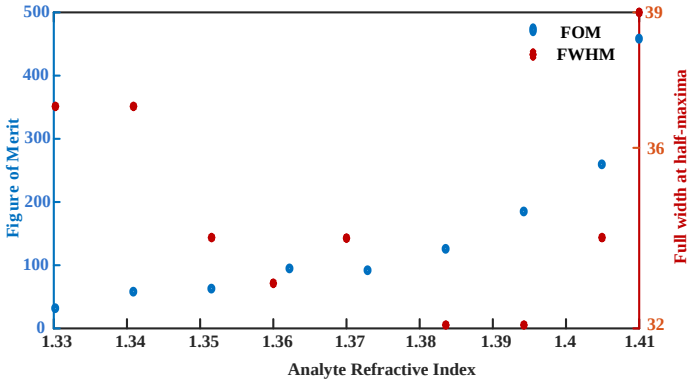

Fig. 6: Variation of figure of merit and full width at half maxima with respect to analyte refractive index.

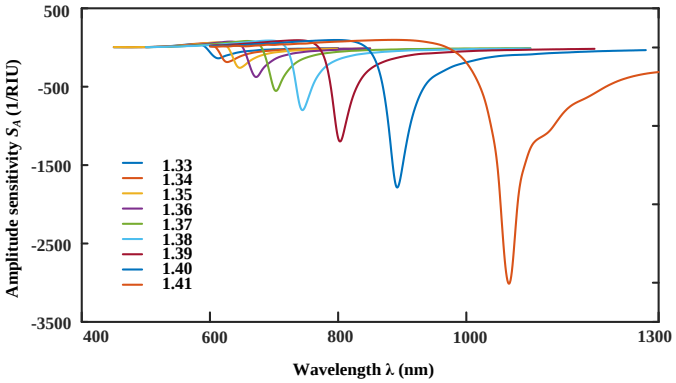

Fig. 7: Amplitude sensitivity spectrum for refractive index of sensing layer (ranging from 1.33 to 1.41).

With a maximum wavelength sensitivity of 18,000 nm/RIU over the analyte refractive index (RI) range of 1.33 to 1.42, the suggested sensor exhibits exceptional wavelength sensitivity. This high sensitivity is attributed to the consistent RI step of 0.01 between analytes within the sensing range. Stronger coupling between the core-guided and surface plasmon modes is indicated by the peak loss gradually increasing with analyte RI. As a result, larger RI values result in improved wavelength sensitivity.

Refractive index resolution, another fundamental performance indicator, is calculated using eq. 5, where the minimum detectable wavelength shift $\Delta\lambda_{min}$ is assumed to be 0.1 nm. Based on this, the sensor achieves a resolution of 5.6×10^{-6} RIU, indicating its ability to detect very subtle changes in analyte RI on the order of 10^{-6}.

$$R = \partial n_a \times \partial \lambda_{min} / \partial \lambda_{peak} \; RIU \qquad \text{eq. 5}$$

Table 1 shows the principal performance parameters, encompassing resonance wavelength, peak loss, wavelength sensitivity, amplitude sensitivity, sensor resolution, FWHM, and FOM, for each analyte refractive index examined in the study.

Table 1. Evaluated sensing performance of the proposed sensor for analyte refractive indices from 1.33 to 1.42.

Analyte RI	Resonance wavelength (nm)	Maximum Loss (dB/cm)	Wavelength Sensitivity (nm/RIU)	Resolution (RIU)	Amplitude Sensitivity (RIU^{-1})	FWHM	FOM
1.33	590	6	1000	1.0×10^{-04}	138	37	27
1.34	600	8	2000	5.0×10^{-05}	138	37	54
1.35	620	8	2000	5.0×10^{-05}	259	34	59
1.36	640	10	3000	3.3×10^{-05}	376	33	92
1.37	670	13	3000	3.3×10^{-05}	554	34	89
1.38	700	23	4000	2.5×10^{-05}	799	32	124
1.39	740	32	6000	1.7×10^{-05}	1199	32	185
1.4	800	46	9000	1.1×10^{-05}	1786	34	262
1.41	890	71	18000	5.6×10^{-06}	3012	39	458
1.42	1070	147	*NA*	*NA*	*NA*	50	NA

Furthermore, the proposed biosensor outperforms several previously reported PCF-SPR sensors, as shown in Table 2, with significantly enhanced wavelength and amplitude sensitivities, along with superior RI resolution.

Table 2. Comparative performance analysis of the proposed sensor with previously reported surface plasmon resonance sensors.

Ref.	Structure of the SPR sensor	RI range	Wavelength sensitivity (nm/ RIU)	Amplitude sensitivity (RIU^{-1})	Resolution (RIU)
[20]	Gold-coated Spiral PCF	1.33–1.38	4300	420.4	2.17×10^{-5}
[18]	Graphene layer on copper	1.33-1.37	2000	140	5.0×10^{-5}
[21]	Au-coated dual-core PCF	1.33-1.40	16000	2255	6.25×10^{-5}
[8]	Au-coated SPR-PCF	1.34-1.37	9000	318	1.10×10^{-5}
[10]	Nb-Au nanofilm SPR	1.36-1.40	8000	1560	8.64×10^{-5}
[11]	Dual-core PCF	1.33-1.41	11500	636	8.70×10^{-6}
[22]	Dual-polarized Decentering Core	1.33-1.39	15,400	852	7.30×10^{-6}
[23]	U-Grooved Selectively Coated	1.29-1.40	12,500	1189	8.0×10^{-6}
[24]	Gold Coated Twin Core PCF	1.28-1.42	9,000	3746	1.0×10^{-6}
[25]	Annularly Arranged Air Hole PCF	1.28-1.40	17,000	605	5.88×10^{-6}
This work	Proposed Monocore PCF	1.33-1.42	18,000	3012	5.6×10^{-6}

To evaluate the fabrication tolerance of the sensor, key structural parameters, pitch, and air-holes (both small air hole and large air hole) diameter were varied from ±2% to ±5% around their optimised values as shown in Fig. 8. The simulation results indicate minimal variation in the loss spectrum and no noticeable shift in the resonance wavelength. The confinement loss at resonant wavelength (590 nm) is found to be 6.40 dB/cm for RI value of 1.33. As it can be seen from the Fig. 8(a), the pitch is increased by 2% (2.04 µm) and then by 5% (2.1 µm) above the optimum value, which results in confinement loss varying from 6.04 dB/cm to 5.46 dB/cm, respectively. Then the pitch is decreased by 2% (1.96 µm) and then by 5% (1.90 µm) below the optimum level, which results in the loss increasing to 6.84 dB/cm and 7.58 dB/cm, respectively. Similarly, we have varied the size of the large air hole, d_1 ($0.8\times\Lambda$), from +5% to – 5% in Fig. 8(b), and a negligible change in loss (6.39 dB/cm to 6.41 dB/cm) is observed. Lastly, we varied the size of small air hole d_2, from +5% to -5% of the optimum value ($0.3\times\Lambda$) in Fig. 8(c). The variation in peak loss is found to be 6.22 dB/cm to 6.59 dB/cm. Because of the variations of all three parameters, the loss slightly varies, but resonant wavelengths are nearly constant for all variations. This stability implies that the sensor's wavelength sensitivity remains unaffected by small deviations in geometric parameters, confirming the design's robustness and manufacturability.

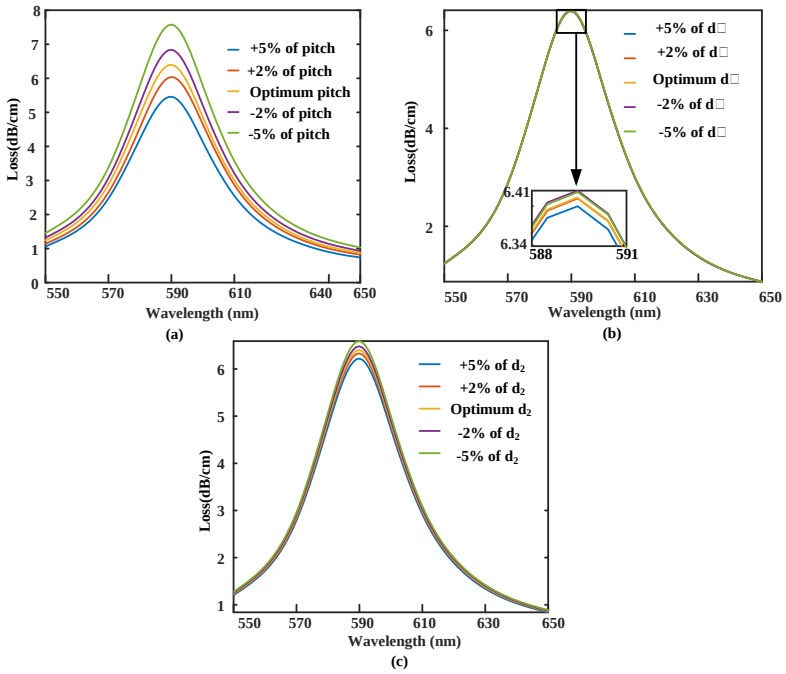

Fig. 8. Effect of modifying structural parameters on sensor characteristics: (a) pitch (Λ), (b) diameter of larger air holes (d_1), and (c) diameter of smaller air holes (d_2).

Conclusion: A monocore photonic crystal fiber (PCF) sensor leveraging surface plasmon resonance (SPR) for the efficient detection of chemical and biological analytes is presented in this paper. The simulation results confirm the 2D cross section geometry achieves a remarkable resolution of 5.6×10^{-6} RIU while functioning efficiently over a refractive index range from 1.33 to 1.42. With a figure of merit (FOM) of 458 RIU^{-1}, an amplitude sensitivity of 3012 RIU^{-1}, and a maximum wavelength sensitivity of 18,000 nm/RIU, it exhibits exceptional performance. Because the sensor construction is built on a standard hexagonal lattice with a single core, it can be easily fabricated using the traditional stack-and-draw method. All these significant characteristics make the sensor as a robust and suitable candidate for real-time biochemical and biomedical sensing applications.

References:

[1] R.H. Ritchie, Plasma losses by fast electrons in thin films, Phys. Rev. 106 (1957) 874–881.
[2] E. Kretschmann, H. Raether, Radiative decay of non-radiative surface plasmons excited by light, Z. Naturforsch. A 23 (1968) 2135–2136.
[3] J. Lv, et al., Recent advances of optical fiber biosensors based on surface plasmon resonance: sensing principles, structures, and prospects, Sens. Diagn. 3 (2024) 1369–1391.
[4] A. Ramola, A.K. Shakya, V. Kumar, A. Bergman, Recent advances in photonic crystal fiber-based SPR biosensors: design strategies, plasmonic materials, and applications, Micromachines 16 (2025) 7.
[5] J. Homola, Surface plasmon resonance sensors for detection of chemical and biological species, Chem. Rev. 108 (2008) 462–493.
[6] Md. Hasan, S. Akter, A. Rifat, S. Rana, S. Ali, A highly sensitive gold-coated photonic crystal fiber biosensor based on surface plasmon resonance, Photonics 4 (2017) 18.
[7] X. Li, S. Li, X. Yan, D. Sun, Z. Liu, T. Cheng, High sensitivity photonic crystal fiber refractive index sensor with externally gold-coated layer based on surface plasmon resonance, Micromachines 9 (2018) 12.
[8] S. Chakma, M.A. Khalek, B.K. Paul, K. Ahmed, M.R. Hasan, A.N. Bahar, Gold-coated photonic crystal fiber biosensor based on surface plasmon resonance: design and analysis, Sens. Bio-Sens. Res. 18 (2018) 7–12.
[9] X. Zhou, T. Cheng, S. Li, T. Suzuki, Y. Ohishi, Practical sensing approach based on surface plasmon resonance in a photonic crystal fiber, OSA Contin. 1 (2018) 1332–1340.
[10] Md. R. Hasan, S. Akter, K. Ahmed, D. Abbott, Plasmonic refractive index sensor employing niobium nanofilm on photonic crystal fiber, IEEE Photonics Technol. Lett. 30 (2018) 315–318.
[11] A.K. Paul, A.K. Sarkar, A. Khaleque, Dual-core photonic crystal fiber plasmonic refractive index sensor: a numerical analysis, Photonic Sens. 9 (2019) 151–161.
[12] S. Sarker, D. Vigneswaran, F. Studnička, Design of a nanoscale gold-coated photonic crystal fiber biosensor, Front. Phys. 11 (2023) 1164255.
[13] D.M. Chow, S.R. Sandoghchi, F.R.M. Adikan, Fabrication of photonic crystal fibers, in: Proc. IEEE 3rd Int. Conf. Photonics, IEEE, 2012, pp. 227–230.
[14] J.C. Knight, T.A. Birks, P. St. J. Russell, D.M. Atkin, All-silica single-mode optical fiber with photonic crystal cladding, Opt. Lett. 21 (1996) 1547.
[15] R. Malabi, et al., Growth and characterisation of gold thin film layer using an e-beam evaporation system for surface plasmon resonance applications, in: Plasmonics in Biology and Medicine XVI, SPIE, 2019, pp. 183–187.

[16] I.H. Malitson, Interspecimen comparison of the refractive index of fused silica, J. Opt. Soc. Am. 55 (1965) 1205–1209.
[17] A.D. Rakić, A.B. Djurišić, J.M. Elazar, M.L. Majewski, Optical properties of metallic films for vertical-cavity optoelectronic devices, Appl. Opt. 37 (1998) 5271–5283.
[18] A.A. Rifat, et al., Copper–graphene-based photonic crystal fiber plasmonic biosensor, IEEE Photonics J. 8 (2016) 1–8.
[19] A.A. Rifat, G.A. Mahdiraji, Y.M. Sua, R. Ahmed, Y.G. Shee, F.R.M. Adikan, Highly sensitive multi-core flat fiber surface plasmon resonance refractive index sensor, Opt. Express 24 (2016) 2485–2495.
[20] M.R. Hasan, et al., Spiral photonic crystal fiber-based dual-polarized surface plasmon resonance biosensor, IEEE Sens. J. 18 (2018) 133–140.
[21] T. Ahmed, A.K. Paul, M.S. Anower, S.M.A. Razzak, Surface plasmon resonance biosensor based on hexagonal lattice dual-core photonic crystal fiber, Appl. Opt. 58 (2019) 8416–8422.
[22] A.M.T. Hoque, A. Islam, F. Haider, H.A. Bin Abdul Rashid, R. Ahmed, R.A. Aoni, Dual-polarized surface plasmon resonance refractive index sensor via decentering propagation-controlled core, Opt. Contin. 1 (2022) 1474.
[23] A.M.T. Hoque, K.F. Al-Tabatabaie, Md. E. Ali, A.M. Butt, S.S.I. Mitu, K.K. Qureshi, U-grooved selectively coated highly sensitive PCF-SPR sensor for broad-range analyte refractive index detection, IEEE Access 11 (2023) 74486–74499.
[24] Md. R. Sardar, M. Faisal, Numerical analysis of highly sensitive twin-core gold-coated D-shaped photonic crystal fiber-based surface plasmon resonance sensor, Sensors 23 (2023) 5029.
[25] N. Tasnim, Md. A. Rahman, Md. R. Rahman, T. Ahmed, Highly sensitive photonic crystal fiber-based surface plasmon resonance biosensor for wide-range organic solution detection, Sens. Bio-Sens. Res. 43 (2024) 100623.